VIP Carbon Materials Very Important Paper

International Edition: DOI: 10.1002/anie.201608453
German Edition: DOI: 10.1002/ange.201608453

A Rapid Microwave-Assisted Thermolysis Route to Highly Crystalline Carbon Nitrides for Efficient Hydrogen Generation

Yufei Guo, Jing Li, Yupeng Yuan, Lu Li, Mingyi Zhang, Chenyan Zhou, and Zhiqun Lin**

Abstract: *Highly crystalline graphitic carbon nitride (g-C_3N_4) with decreased structural imperfections benefits from the suppression of electron–hole recombination, which enhances its hydrogen generation activity. However, producing such g-C_3N_4 materials by conventional heating in an electric furnace has proven challenging. Herein, we report on the synthesis of high-quality g-C_3N_4 with reduced structural defects by judiciously combining the implementation of melamine–cyanuric acid (MCA) supramolecular aggregates and microwave-assisted thermolysis. The g-C_3N_4 material produced after optimizing the microwave reaction time can effectively generate H_2 under visible-light irradiation. The highest H_2 evolution rate achieved was 40.5 $\mu mol\,h^{-1}$, which is two times higher than that of a g-C_3N_4 sample prepared by thermal polycondensation of the same supramolecular aggregates in an electric furnace. The microwave-assisted thermolysis strategy is simple, rapid, and robust, thereby providing a promising route for the synthesis of high-efficiency g-C_3N_4 photocatalysts.*

Among various renewable energy sources, solar production of hydrogen (H_2) fuel through photocatalytic water splitting is widely recognized as an ideal route to utilizing solar energy as both solar energy and water are highly abundant on Earth. Of the various materials that have been reported for active H_2 generation under UV and visible-light irradiation,[1–8] graphitic carbon nitride (g-C_3N_4) has garnered much attention as it is a highly active and stable photocatalyst for H_2 generation upon exposure to visible light.[9–11] To date, several nitrogen-rich molecules, such as dicyandiamide, melamine, and urea, have been routinely used as precursors to produce g-C_3N_4 at high temperatures (400–600 °C) in air or inert atmosphere.[9,10] Notably, these N-rich molecules can follow several reaction pathways with the formation of various intermediates during the polycondensation of g-C_3N_4.[9,10] The characterization of g-C_3N_4 reveals the presence of structural defects that are due to incompletely reacted intermediates, including amino and/or cyano groups.[12,13] The photocatalytic activity is sensitively affected by these structural defects because they can serve as charge trap sites in photocatalytic reactions. To address this issue, one strategy is to avoid the complicated reaction pathways, thus reducing the formation of intermediate products during the polycondensation into g-C_3N_4. The second strategy involves the preparation of highly crystalline g-C_3N_4 to reduce the number of structural defects. It is noteworthy that the conventional synthetic approach, which involves heating in an electric furnace, cannot yield high-quality g-C_3N_4 as noted above. Clearly, an effective synthetic strategy for the synthesis of highly crystalline g-C_3N_4 is desirable yet challenging.

Compared with single-component N-rich precursors, the advantages of using supramolecular aggregates as starting materials for creating g-C_3N_4 are twofold. First, the supramolecular aggregates possess a preorganized network that is structurally similar to the local arrangement in g-C_3N_4 building blocks at the molecular level. Second, because of the hydrogen-bonded supramolecular structure, the supramolecular aggregates reduce the sublimation of the N-rich molecules (e.g., melamine) during polycondensation at elevated temperatures.[14,15] Consequently, g-C_3N_4 samples obtained from supramolecular aggregates as starting precursors benefit from reduced structural defects and enhanced photocatalytic H_2 generation.[14,15]

Herein, we report on a simple route for the synthesis of highly crystalline g-C_3N_4 with a significantly reduced number of defects for high-efficiency H_2 generation by judiciously combining the use of melamine–cyanuric acid supramolecular aggregates with rapid, microwave-assisted thermolysis. 1,3,5-Triazine-2,4,6-triol, a planar molecule with carbonyl groups at each vertex (compound **2** in Figure 1) was complexed with melamine (**1**) to produce hydrogen-bonded melamine–cyanuric acid (MCA) supramolecular aggregates (**3**). Intriguingly, the MCA supramolecular aggregates possess structural similarity to g-C_3N_4 (**4**). They can thus be directly polymerized to yield g-C_3N_4, thereby eliminating the complicated reaction pathways involved in the formation of intermediates and producing g-C_3N_4 with greatly reduced defects. Moreover, in sharp contrast to the conventional approach based on heating in an electric furnace, the microwave-assisted thermolysis approach enables the production of g-C_3N_4 within minutes with greatly improved crystallinity owing to the strong rotation, friction, and collision of N-rich molecules under microwave irradiation.[16–18] The photocatalytic H_2 generation rate of a g-C_3N_4 sample thus obtained was two times higher

[*] Y. Guo, J. Li, Dr. Y. Yuan, C. Zhou
School of Chemistry and Chemical Engineering
Anhui University
Hefei 230601 (P. R. China)
E-mail: yupengyuan@ahu.edu.cn
L. Li, Dr. M. Zhang
School of Physics and Electronic Engineering
Harbin Normal University
Harbin 150025 (P. R. China)
Dr. Y. Yuan, Prof. Z. Lin
School of Materials Science and Engineering
Georgia Institute of Technology
Atlanta, GA 30332 (USA)
E-mail: zhiqun.lin@mse.gatech.edu

Supporting information for this article can be found under: http://dx.doi.org/10.1002/anie.201608453.

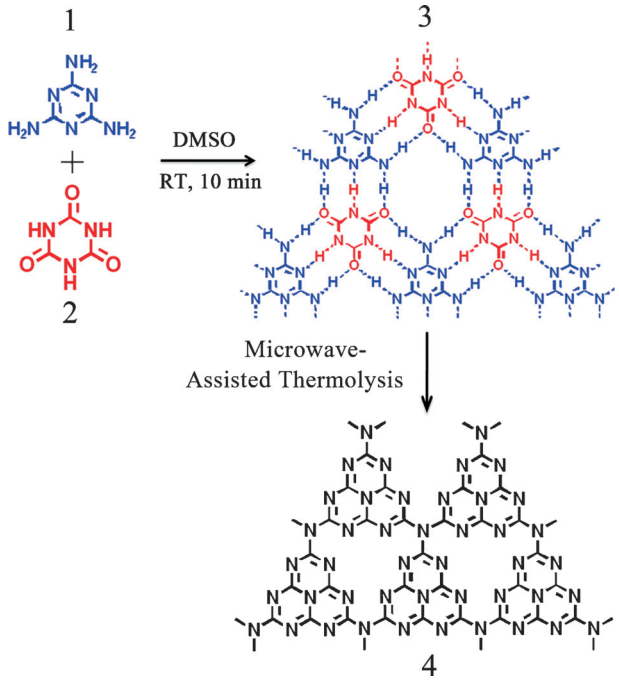

Figure 1. g-C_3N_4 formation. Molecular structures of melamine (**1**), cyanuric acid (**2**), MCA supramolecular aggregates (**3**), and g-C_3N_4 (**4**).

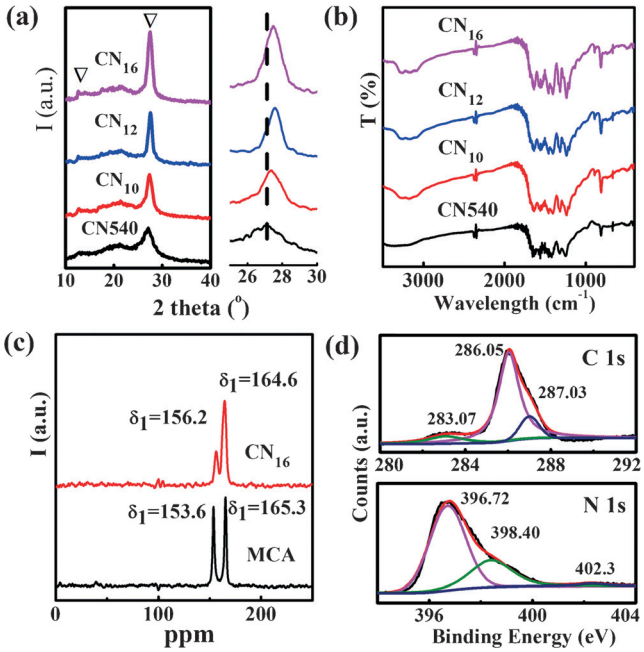

Figure 2. a) XRD patterns and b) FTIR spectra of CN_t samples produced by microwave-assisted thermolysis of MCA precursors for 10, 12, and 16 min, respectively. The XRD pattern and FTIR spectrum of a reference sample (CN540) prepared by heating MCA precursors at 540 °C for 4 h are also provided for comparison. The right panel in (a) shows close-up XRD patterns of g-C_3N_4 samples from $2\theta = 25$–$30°$. c) ^{13}C MAS NMR spectra of MCA supramolecular aggregates and CN_{16}. d) XPS spectra showing the binding energies of C 1s and N 1s for the CN_{16} sample.

than that of a g-C_3N_4 sample obtained by polymerizing MCA supramolecular aggregate in an electric furnace.

Specifically, MCA supramolecular aggregates (**3**) were precipitated from an equimolar mixture of melamine and cyanuric acid in dimethyl sulfoxide (DMSO). The MCA aggregates possess a spherical morphology with an average size of about 3 μm, as shown by scanning electron microscopy (SEM; see the Supporting Information, Figure S1 a). Further analysis of the MCA spheres revealed that they are composed of closely assembled nanoparticles with an average size of 200 nm or smaller (Figure S1 b). The intense peaks at $2\theta = 10°$ and 28° in the XRD pattern were attributed to the periodic arrays of intraplanar stacking and interlayer aromatic stacking of MCA, respectively (Figure S2). Compared to g-C_3N_4, with peaks located at $2\theta = 13°$ and 27.5° as described below (Figure 2 a), the different peak positions of MCA ($2\theta = 10°$ and 28°) may be due largely to the hydrogen-bonded network in MCA (**3**). Nonetheless, this XRD result further substantiated that the structure of MCA (**3**) bears a strong resemblance to g-C_3N_4 (**4**).

Subsequently, the MCA supramolecular aggregates were thermalized for various periods of time using the microwave-assisted heating strategy (see the Experimental Section in the Supporting Information). CuO was used as the microwave absorber as it can intensely and effectively absorb microwaves to increase the temperature up to 1285 K in less than 7 min.[19] The resulting products were labeled CN_t, where t is the microwave heating time in minutes. A control sample was also prepared by polymerizing the MCA supramolecular aggregates at 540 °C for 4 h in Ar atmosphere by conventional heating in an electric furnace (CN540). After 10 min polycondensation by microwave irradiation (yielding CN_{10}), the products showed the yellow color typical of g-C_3N_4. The XRD pattern of CN540 is essentially the same as that reported in the literature.[20] The two characteristic diffraction peaks at $2\theta = 13°$ and 27.5° (▽) correspond to the periodic in-plane tri-*s*-triazine stacking and the interlayer structural aromatic packing, respectively (Figure 2 a).[16,21] The wide diffraction peak of the CN540 sample suggested that low-crystalline g-C_3N_4 was produced by conventional heating. It is interesting to note that in spite of the different heating process with microwave-assisted heating of MCA for only 8 min, the CN_8 sample showed essentially the same XRD pattern as MCA with the emergence of a new diffraction peak at $2\theta = 12°$, indicating the polymerization of melamine and cyanuric acid (Figure S2). Importantly, the CN_{10} sample obtained after microwave-assisted thermolysis for 10 min displayed two distinct diffraction peaks at $2\theta = 13°$ and 27.5°, reflecting that g-C_3N_4 had been formed after microwave-assisted heating for 10 min. Moreover, in comparison to the XRD pattern of the CN540 sample with a broad and weak peak at $2\theta = 27.5°$, a relatively intense and narrower diffraction peak was observed in the CN_{10} sample, indicating improved crystallinity. Prolonged reaction times of 12 and 16 min yielded g-C_3N_4 (CN_{12} and CN_{16}) with progressively increasing diffraction peak intensities (Figure 2 a). We note that the 27.5° peak was shifted to a higher angle with increased reaction time (Figure 2 a, right), suggesting a decreased interlayer distance in the resulting CN_{12} and CN_{16} samples. Clearly, the increased XRD peak intensity and the decreased interlayer

distance upon increasing the reaction time revealed that the polycondensation of the MCA precursors is enhanced by microwave-assisted thermolysis, resulting in highly crystalline g-C_3N_4.

FTIR measurements were performed to analyze the MCA polycondensation at different microwave reaction times (Figure 2b). The white CN_8 sample gave rise to several bands at 3396, 3232, 1748, 1652, 1535, 1450, 1074, 1025, 910, 810, and 765 cm^{-1}, corresponding to the MCA supramolecular aggregates (Figure S3). The increased intensity of these peaks in CN_8 is indicative of the polycondensation of MCA; this is particularly true for the enhanced peak at 810 cm^{-1}, a signature of the formation of tri-*s*-triazine (Figure S3).[14] In the CN_{10} sample, the characteristic peaks of the MCA precursors have disappeared, and new peaks have emerged at 810, 1240, 1318, 1411, 1460, 1568, and 1640 cm^{-1}, which belong to the stretching vibrations of the CN heterocycles,[16] signifying the formation of tri-*s*-triazine.[16] The intensity of these peaks increased as the polycondensation reaction progressed (from CN_{10} to CN_{12} to CN_{16}). The NH_2 stretching vibration mode was observed at approximately 3200 cm^{-1}.

The structure of the CN_{16} sample was further investigated by ^{13}C MAS NMR spectroscopy (Figure 2c). The NMR spectrum showed two resolved resonances at $\delta_1 = 156.2$ and $\delta_2 = 164.6$ ppm, corresponding to the C(i) atoms in the CN_3 groups and the C(e) atoms in $CN_2(-NH_2)C$, respectively (Figure S4). The ^{13}C MAS NMR spectrum clearly corroborated the g-C_3N_4 frameworks in CN_{16}.[16] Notably, the MCA supramolecular aggregates also displayed two resonances at $\delta_1 = 153.6$ and $\delta_2 = 165.3$ ppm, corroborating the structural similarity to CN_{16} (Figure 2c).

To further investigate the structural details of CN_{16}, samples were analyzed by X-ray photoelectron spectroscopy (XPS; Figure 2d). The XPS analysis confirmed the presence of carbon and nitrogen in CN_{16} (Figure S5). The O 1s peak is due to doped cyanuric acid (Figure S5). The carbon species with a binding energy of 286.05 eV arises from the $C(sp^2)$=N bonds in the *s*-triazine rings. The peak at 283.07 eV is a result of the graphitic carbon while the peak at 287.03 eV is due to C–O bonds. The N 1 s binding energy can be deconvoluted into three peaks of 396.72, 398.40, and 402.32 eV (Figure 2d).[21,22] The strongest N 1s peak at 396.72 eV corresponds to sp^2-hybridized aromatic N atoms (C=N–C) in the *s*-triazine rings. The N 1s peak at 398.4 eV is indicative of amino groups (C–N–H), which is consistent with the FTIR measurements (Figure 2b). The weakest N 1s peak at 402.32 eV is due to the charging effect.[14,23]

Elemental analysis revealed the C/N molar ratios of CN540, CN_{10}, CN_{12}, and CN_{16} to be 0.674, 0.671, 0.679, and 0.684, respectively. The nitrogen richness of the g-C_3N_4 samples arises from the dangling NH_2 groups in g-C_3N_4, as revealed by FTIR spectroscopy. Although the measured C/N molar ratios are lower than the theoretical ratio of 0.75 for g-C_3N_4, the progressively increasing C/N ratios clearly reflect the improved structural integrity of the CN_i samples. We note that the suite of characterizations discussed above substantiate the rapid and effective formation of g-C_3N_4 by microwave-assisted thermolysis of MCA supramolecular aggregates.

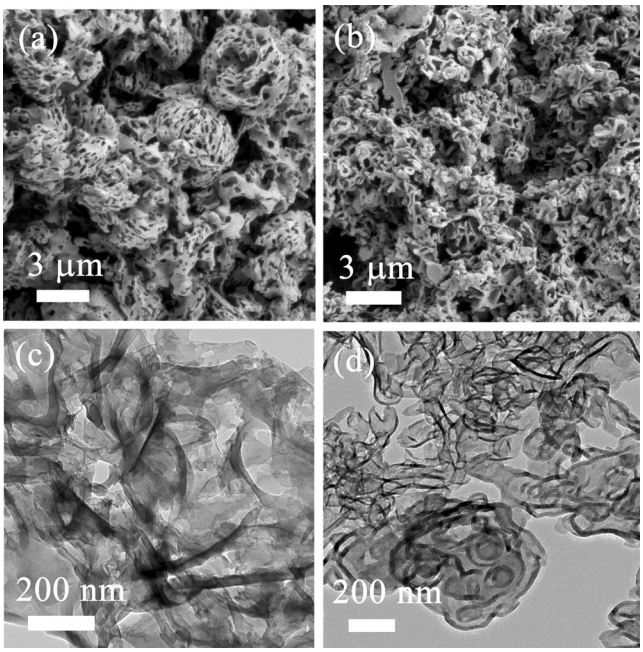

Figure 3. SEM images of a) CN540 and b) CN_{16}. TEM images of c) CN540 and d) CN_{16}. Whereas CN540 has a sphere-like morphology, CN_{16} has an irregular morphology resulting from the collapse of the MCA sphere precursors. Moreover, the CN_{16} nanosheets are thinner than those of CN540.

Figure 3 shows representative SEM and TEM images of CN_{16} and CN540 samples. The CN540 sample displayed a loose and porous sphere-like morphology with an average sphere size of about 4 μm (Figure 3a). The overall appearance of CN540 resembles that of the MCA precursors. Interestingly, the CN540 spheres are composed of velvet-like nanosheets with a thickness of less than 30 nm (Figure 3c). In contrast, the CN_{16} sample exhibited an irregular morphology. Obviously, the MCA spheres shown in Figure S1 had completely collapsed after microwave-assisted heating for 16 min (Figure 3b), which is due to the large amount of gases, such as NH_3, spontaneously generated during the polycondensation of the MCA supramolecular aggregates. The quick escape of gases led to the formation of highly fluffy and porous structures. The g-C_3N_4 nanosheets produced by microwave-assisted heating were also further visualized by TEM (Figure 3d).

UV/Vis absorption spectra of g-C_3N_4 samples produced by microwave-assisted heating for different periods of time (CN_{10}, CN_{12}, and CN_{16}) and the control example (CN540) are shown in Figure S6. The band gap of the CN_{16} sample was estimated to be 2.7 eV based on the onset of the absorption edge.[16] It is noticeable that the intensity of the absorption in the visible region increased with the microwave reaction time.

The effective transfer of photogenerated charge carriers depends sensitively on the trap sites in the semiconductor, which are closely related to the structural defects of the material. In this context, the steady-state photoluminescence (PL) upon excitation at 350 nm was measured in order to study the charge recombination in g-C_3N_4. As shown in Figure 4a, the CN540 sample gave rise to a strong emission

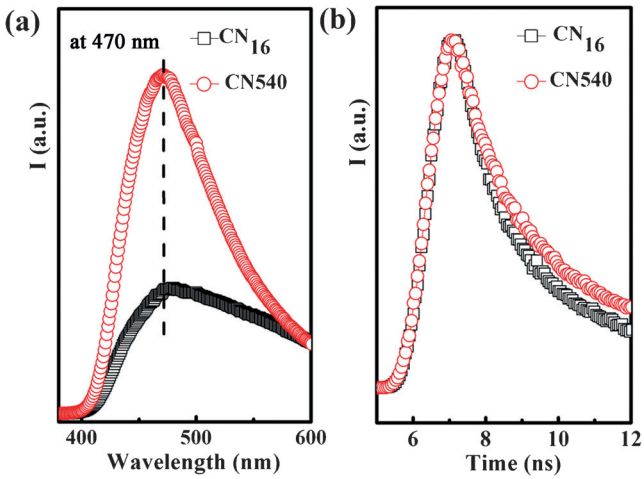

Figure 4. a) Steady-state PL spectra and b) time-resolved PL spectra of CN_{16} and CN540 samples. The quenching of the PL intensity in the CN_{16} sample signifies the reduced structural defects within the framework. In addition, the shorter lifetime in CN_{16} indicates that charge transfer is more rapid than in the CN540 sample.

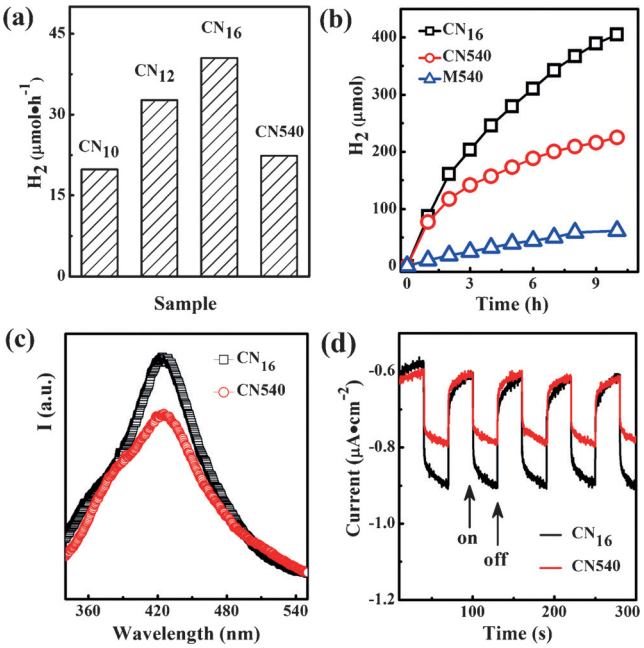

Figure 5. a) Photocatalytic H_2 generation rates of CN_t and CN540 samples. b) H_2 generation with CN_{16}, CN540, and M540 samples as a function of time. The M540 sample was prepared by polycondensation of melamine alone at 540 °C for 4 h in Ar. c) Photoluminescence spectra of TAOH formed by the reaction of TA with ·OH radicals generated from CN_{16} and CN540 samples under visible-light irradiation for 10 min. d) Transient photocurrent response of ITO/CN_{16} and ITO/CN540 at −1.0 V vs. Ag/AgCl in 0.5 M Na_2SO_4 exposed to visible light ($\lambda \geq 420$ nm, 300 W Xe lamp).

peak centered at 470 nm. In contrast, a significantly smaller emission peak was observed for CN_{16}, suggesting decreased recombination of photogenerated electron–hole pairs. This observation further supported the reduced structural defects in the CN_{16} sample as defects commonly serve as electron–hole recombination centers. More importantly, the improved crystallinity of the CN_t samples (Figure 2a) resulted in rapid charge transfer in the CN_{16} sample compared to CN540, as confirmed by time-resolved PL spectroscopy measurements (Figure 4b). The average PL lifetimes of CN540 and CN_{16} were 3.96 and 2.79 ns, respectively. The shorter lifetime of the charge carriers in CN_{16} signifies the rapid transfer of photogenerated electron–hole pairs involved in the redox reaction for CN_{16}, thereby potentially promoting the photocatalytic H_2 production.[24]

Visible-light-induced photocatalytic H_2 generation was then attempted by capitalizing on the produced g-C_3N_4 samples (20 mg) in the presence of triethanolamine (TEOA) as the sacrificial electron donor. Pt (0.5 wt%) was photoloaded in situ onto all g-C_3N_4 samples as a co-catalyst to boost H_2 generation. Control experiments showed that no H_2 generation occurred in the absence of either photocatalyst or light irradiation, confirming that H_2 generation requires both light irradiation and a g-C_3N_4 photocatalyst. The photocatalytic H_2 generation rate of CN_{10} was determined to be 19.8 μmol h^{-1}, which is comparable to that of a CN540 sample (22.4 μmol h^{-1}; Figure 5a). Notably, the g-C_3N_4 sample prepared by polycondensation of melamine alone at 540 °C for 4 h in Ar in an electric furnace (M540) only showed a H_2 generation rate of 6 μmol h^{-1} under the same experimental conditions. This result clearly demonstrates the advantage of using the MCA supramolecular aggregates as precursors instead of melamine alone to create g-C_3N_4. The photocatalytic H_2 generation activity was even higher with the CN_t samples with increased microwave reaction times. The highest H_2 evolution rate of 40.5 μmol h^{-1} was achieved with the CN_{16} sample; this value is nearly two times larger than that of the CN540 sample and more than six times larger than that of the M540 sample. The H_2 evolution rate of 40.5 μmol h^{-1} is relatively high as the specific surface area of CN_{16} (45.3 $m^2 g^{-1}$) is 1.5 times smaller than that of CN540 (68.3 $m^2 g^{-1}$), which further substantiates the effectiveness of the present microwave-assisted thermolysis strategy for high-quality g-C_3N_4 production. Interestingly, the initial H_2 generation rates of CN_{16} and CN540 were essentially the same during the first hour (Figure 5b). As the microwave reaction time was increased, the H_2 generation rate was comparatively reduced for the CN540 sample, revealing the enhanced stability of the CN_{16} sample for photocatalytic H_2 generation, which is a direct consequence of the improved crystallinity of the CN_t samples as determined by XRD (Figure 2a).

As noted above, the enhanced photocatalytic H_2 production can be ascribed to the reduced structural defects and the improved crystallinity of the CN_t samples and thus the decreased number of trap sites in g-C_3N_4 for efficient separation of photogenerated electron–hole pairs. To confirm the effectiveness of the charge separation, we carried out ·OH radical concentration measurements. As the ·OH radicals can oxidize terephthalic acid (TA) to 2-hydroxyterephthalic acid (TAOH), which has a strong emission peak at 426 nm,[25,26] the fluorescence intensity of TAOH can be used to monitor the charge separation efficiency. Compared to the CN540 sample, the higher fluorescence intensity of TAOH (Figure 5c) in the CN_{16} sample revealed that more holes in the excited CN_{16} sample are involved in the oxidation reaction of TA than in

the CN540 sample, indicating the more effective charge separation in CN_{16} compared to CN540.

We measured the transient photocurrent in CN_{16} and CN540 samples to further evaluate the efficient separation of electron–hole pairs in the CN_{16} sample (Figure 5d with the dark current subtracted). The photocurrent responses were prompt and reproducible during the on/off cycles of visible-light excitation. Despite the relatively small value, the photocurrent generated in the CN_{16} sample was still comparatively large compared to that in CN540, clearly confirming the effective separation of photoinduced electrons and holes in CN_{16} compared to CN540.

In summary, we have developed a rapid and effective strategy that is based on the microwave-assisted thermolysis of MCA supramolecular aggregates to synthesize highly crystalline g-C_3N_4 with reduced structural defects and enhanced photocatalytic H_2 generation activity under visible-light irradiation. The efficient separation of photogenerated electrons and holes in highly crystalline g-C_3N_4 accounted for the enhanced H_2 generation. This inexpensive microwave-assisted strategy for the thermolysis of precursors and supramolecular aggregates may open possibilities for the targeted design of a broad range of high-efficiency photocatalysts with potential applications in water splitting, photocatalytic degradation of organic pollutants, and photoelectrochemical anticorrosion.

Acknowledgements

This work was financially supported by the National Natural Science Foundation of China (51572003), Anhui Provincial Natural Science Foundation (1508085ME105, 1408085MB22), the Project sponsored by SRF for ROCS, SEM, and Technology Foundation for Selected Overseas Chinese Scholar, Ministry of Personnel of China.

Keywords: graphitic carbon nitride · microwave-assisted thermolysis · photocatalysis · supramolecular aggregates · water splitting

How to cite: *Angew. Chem. Int. Ed.* **2016**, *55*, 14693–14697
Angew. Chem. **2016**, *128*, 14913–14917

[1] A. Fujishima, K. Honda, *Nature* **1972**, *238*, 37–38.
[2] A. Kudo, Y. Miseki, *Chem. Soc. Rev.* **2009**, *38*, 253–278.
[3] X. Chen, S. Shen, L. Guo, S. Mao, *Chem. Rev.* **2010**, *110*, 6503–6570.
[4] Y. Yuan, L. Ruan, J. Barber, S. C. J. Loo, C. Xue, *Energy Environ. Sci.* **2014**, *7*, 3934–3951.
[5] X. Li, J. Yu, M. Jaroniec, *Chem. Soc. Rev.* **2016**, *45*, 2603–2636.
[6] J. Hu, A. Liu, H. Jin, D. Ma, D. Yin, P. Ling, S. Wang, Z. Lin, J. Wang, *J. Am. Chem. Soc.* **2015**, *137*, 11004–11010.
[7] M. Ye, J. Gong, Y. Lai, C. Lin, Z. Lin, *J. Am. Chem. Soc.* **2012**, *134*, 15720–15723.
[8] B. Han, Y. H. Hu, *J. Phys. Chem. C* **2015**, *119*, 18927–18934.
[9] S. Cao, J. Low, J. Yu, M. Jaroniec, *Adv. Mater.* **2015**, *27*, 2150–2176.
[10] S. Ye, R. Wang, M. Wu, Y. Yuan, *Appl. Surf. Sci.* **2015**, *358*, 15–27.
[11] Y. Zheng, L. Lin, B. Wang, X. Wang, *Angew. Chem. Int. Ed.* **2015**, *54*, 12868–12884; *Angew. Chem.* **2015**, *127*, 13060–13077.
[12] Z. Lin, X. Wang, *Angew. Chem. Int. Ed.* **2013**, *52*, 1735–1738; *Angew. Chem.* **2013**, *125*, 1779–1782.
[13] M. K. Bhunia, K. Yamauchi, K. Takanabe, *Angew. Chem. Int. Ed.* **2014**, *53*, 11001–11005; *Angew. Chem.* **2014**, *126*, 11181–11185.
[14] Y. Jun, E. Z. Lee, X. Wang, W. H. Hong, G. D. Stucky, A. Thomas, *Adv. Funct. Mater.* **2013**, *23*, 3661–3667.
[15] M. Shalom, S. Inal, C. Fettkenhauer, D. Neher, M. Antonietti, *J. Am. Chem. Soc.* **2013**, *135*, 7118–7121.
[16] Y. Yuan, L. Yin, S. Cao, L. Gu, G. Xu, P. Du, H. Chai, Y. Liao, C. Xue, *Green Chem.* **2014**, *16*, 4663–4668.
[17] L. Lin, P. Ye, C. Cao, Q. Jin, G. Xu, Y. Shen, Y. Yuan, *J. Mater. Chem. A* **2015**, *3*, 10205–10208.
[18] R. Hoogenboom, U. S. Schubert, *Macromol. Rapid Commun.* **2007**, *28*, 368–386.
[19] K. J. Rao, B. Vaidhyanathan, M. Ganguli, P. A. Ramakrishnan, *Chem. Mater.* **1999**, *11*, 882–895.
[20] X. Wang, K. Maeda, A. Thomas, K. Takanabe, G. Xin, J. M. Carlsson, K. Domen, M. Antonietti, *Nat. Mater.* **2009**, *8*, 76–80.
[21] Y. Yuan, W. Xu, L. Yin, S. Cao, Y. Liao, Y. Tng, C. Xue, *Int. J. Hydrogen Energy* **2013**, *38*, 13159–13163.
[22] Y. Cui, Z. Ding, X. Fu, X. Wang, *Angew. Chem. Int. Ed.* **2012**, *51*, 11814–11818; *Angew. Chem.* **2012**, *124*, 11984–11988.
[23] J. Liu, T. Zhang, Z. Wang, G. Dawson, W. Chen, *J. Mater. Chem.* **2011**, *21*, 14398–14401.
[24] J. Lee, H. S. Shim, M. Lee, J. K. Song, D. Lee, *J. Phys. Chem. Lett.* **2011**, *2*, 2840–2845.
[25] J. Huang, K. Ding, X. Wang, X. Fu, *Langmuir* **2009**, *25*, 8313–8319.
[26] G. Liu, P. Niu, L. Yin, H. Cheng, *J. Am. Chem. Soc.* **2012**, *134*, 9070–9073.

Received: August 29, 2016
Published online: October 6, 2016

